PROCESSING, CHARACTERISATION AND OXIDATION RESISTANCE OF βNiAl BOND COAT: Al AND Zr EFFECTS

A.D. Chandio [a,*], A.A. Shaikh [b], W. Salman [c], H. Ahmed [a]

[a] NED University of Engineering and Technology, Metallurgical Engineering Department, Pakistan
[b] NED University if Engineering and Technology, Faculty of Chemical and Process Engineering, Pakistan
[c] Northwestern Polytechnical University, State key Laboratory of Solidification Processing, School of Material Science and Engineering, China

Abstract

Platinum-modified-βNiAl is a bond coat (BC) material for thermal barrier coatings (TBCs) applications applied on aero-engine hardware to reduce their surface temperatures. However, it is desirable to minimize its production and material costs by the low-cost alternatives of similar performance. It has been acknowledged that the small concentration of the reactive elements (REs), such as Zr, Hf, and Y, could tremendously enhance the oxide adhesion even in some cases better than Pt modified counterparts. The aim of this study was to design and fabricate the Zr-modified-βNiAl bond coat on CMSX-4 superalloy using an aluminizing method. Moreover, the study focused on the development of a systematic understanding of underlying mechanisms behind the beneficial effects of REs. Initially, three sets of BCs were prepared: Zr-free βNiAl (undoped), Al and Zr co-deposited in a single-step process (1SP), and Zr and Al, which were individually deposited in two processing steps (2SP): zirconizing and aluminizing. Such three sets of BCs helped to understand the processing, as well as Zr and Al effects on scale adhesion. In particular, 1SP/2SP BCs showed uniformity of Zr in the form of precipitates and networks that caused hardness enhancement. All BCs were isothermally oxidized at 1150ºC for 100 hours wherein 2SP revealed the best spallation resistance, microstructural stability, and its Zr-oxide pegs were extended to substrates. In addition to the Zr effect, BC Al content was found to affect the oxide adhesion equally. Under identical Zr contents (of 1SP and 2SP = 1at %), the higher Al showed the better spallation resistance while lower Al caused the inverse effect of Zr owing to its reactive nature that was termed as over doping. Moreover, it was established that over-doping either local or into entire BC, accelerated the Al depletion that destabilized the βNiAl into γ'-Ni₃Al phase. An extensive discussion is presented in the light of the observed results.

Keywords: βNiAl bond coat; Oxidation resistance; Thermal barrier coating (TBC); Doping of reactive metals (REs); Aluminizing

1. Introduction

The high-temperature protective nickel aluminide (βNiAl) coatings have been developed and are commonly known as alumina (α-Al_2O_3) forming compounds, which are applied onto turbine blades exposed to oxidative and corrosive environments [1, 2]. Such coatings serve as BC material in thermal barrier coating (TBC) [3-7] systems. The choice of α-Al_2O_3 is based on several factors; for example, its thermodynamic compatibility with TBC, low diffusivity of oxygen, etc. [8]. Therefore, βNiAl based intermetallic are candidate materials for TBC applications. However, they suffer from substrate outward migration and Al in/outward depletion during oxidation subsequently impairing its usefulness for

TBC applications. To overcome such problems and improve the spallation lives of such bond coats, platinum was first incorporated into commercialized βNiAl BCs [9]. Such BCs are still being extensively used as a state-of-art BC in TBC systems [10-12]. In general, PtNiAl improves scale adhesion and high-temperature stability, reduces void formation, promotes selective aluminium depletion, etc.[13-15], but its performance is affected by surface rumpling. Such problems are greatly minimized by recently developed Pt-γ/γ' BCs. Moreover, REs addition into β-PtNiAl and Pt-γ/γ' BCs minimizes the propensity of such type of failures due to REs reducing the scale growth by changing the oxidation mechanism, etc [16]. It is desirable to reduce the BC cost incurred due to platinum incorporation and the adoption of costly

production methods. In this connection, the use of REs had been explored for the past several decades. The commonly acknowledged beneficial effects include: (1) oxide pegging, (2) enhanced plasticity of scale due to its modification, (3) elimination of pores, (4) changing growth mechanisms, and (5) alteration of scale microstructure [17-19]. Therefore, present study aims to deposit the Zr-doped BC by pack process, which is an economical production route compared to PVD and CVD methods for aforementioned BCs. The processing and performance of Zr doped BCs is discussed and their benefits over the Pt modified bond coats are highlighted.

2. Experimental

The aluminide coatings were deposited on the CMSX-4 superalloy substrate having a nominal composition in wt % of 61.42 Ni, 6.40 W, 2.90 Re, 5.64 Al, 1.03 Ti, 6.60 Ta, 9.60 Co, 6.40 Cr, and 0.10 Hf. The alloy coupons were cut into (5x5x2) mm discs, progressively ground to 1200 grit, and ultrasonically cleaned in ethanol. The pack mixtures for aluminising (Al addition) consisted of (in wt %) 15 Al ($\leq$ 30μm) + 1 AlCl$_3$ + 3 NH$_4$Cl + 81 Al$_2$O$_3$, and similarly for zirconizing (Zr doping), the mixture was composed of 10 Zr ($\leq$ 45μm) + 2 ZrCl$_4$ + 3 NH$_4$Cl + 85 Al$_2$O$_3$. Three sets of coatings were prepared, i.e., Zr-free βNiAl, Zr, and Al co-deposited in one step (1SP), and Zr and Al individually deposited in two steps (2SP). The corresponding aluminizing process schematics are presented in Fig. 1a-c, which is self-explanatory. The processing times and temperatures selected for aluminising were 6-10 hours and 950°C, respectively, for all samples. While zirconising time and temperature were 1050°C and 3 hours, respectively. Furthermore, all coated substrates received diffusion treatment at 1100°C for 3 hours that was followed by annealing treatment for 5 hours at 900°C (Fig. 1d), which was one of the unique features of the methodology presented here. Finally, isothermal oxidation tests were carried out using Setaram thermo-balance at 1150°C for 100 hours to analyse the growth rates in terms of weight gains. For further investigation of the phases present in the coating, their microstructural evolution and chemistry were examined. The techniques used were scanning electron microscopy (SEM, FEG XL30 using 20 kV) attached with energy-dispersive X-ray spectroscopy (EDX) using both secondary electron (SE) and backscattered electron (BSE) modes, X-ray fluorescence spectroscopy (XRF), X-ray diffraction (XRD), Photoluminescence piezo-spectroscopy (PLPS), and CSM nano-indenter to investigate mechanical properties of the coating, such as hardness and elastic modulus.
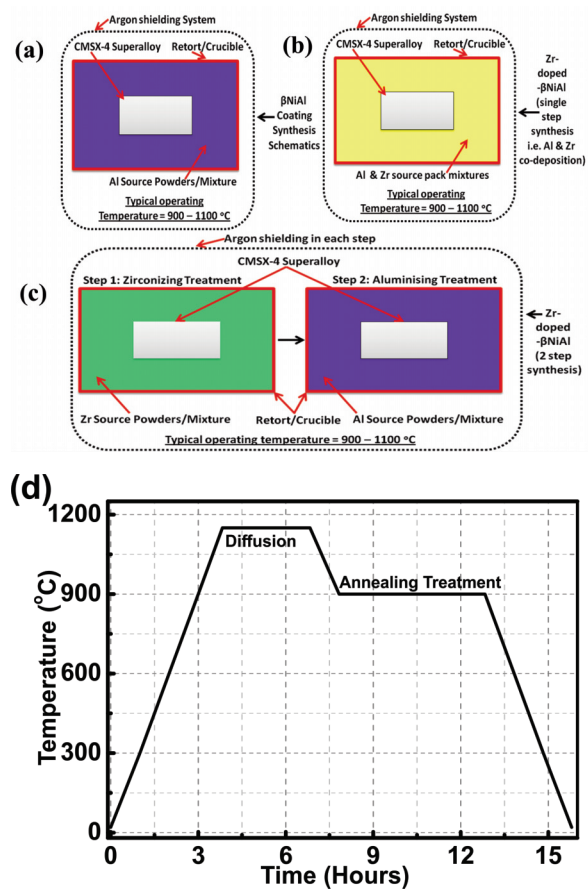

Figure 1. Pack aluminising schematics and diffusion cycles; (a) Zr-free βNiAl, (b) 1SP (Zr & Al co-deposited), (c) 2SP (Zr & Al individually deposited), and (d) diffusion-annealing temperature cycle

3. Results
3.1. As-deposited BCs
3.1.1. Microstructures, Phases & Chemistry

Fig. 2 represents cross-sections and surface microstructures of Zr-free, 1SP, and 2SP BCs, respectively. The characteristic two layers, i.e. outer βNiAl and inner IDZ were shown in all samples. The white particles in the undoped sample appearing either in βNiAl layer cross-sections (Fig. 2a) or on its surface (Fig. 2b) were typical Cr-rich ppts (see Table 1). To understand the dopant distribution, both doped 1SP and 2SP BCs cross-sections were divided into three zones. In both doped BCs, Zr was observed to be soluble in zone 1, while zones 2 and 3 showed its distribution into white contrasted ppts and networks, as shown in Fig. 2 (c) and (e). While surface examination showed Zr distribution in lumps or extended particles (nonuniform) for 1SP (Fig. 2d), the 2SP surface exhibited finely distributed Zr particles (Fig. 2f).
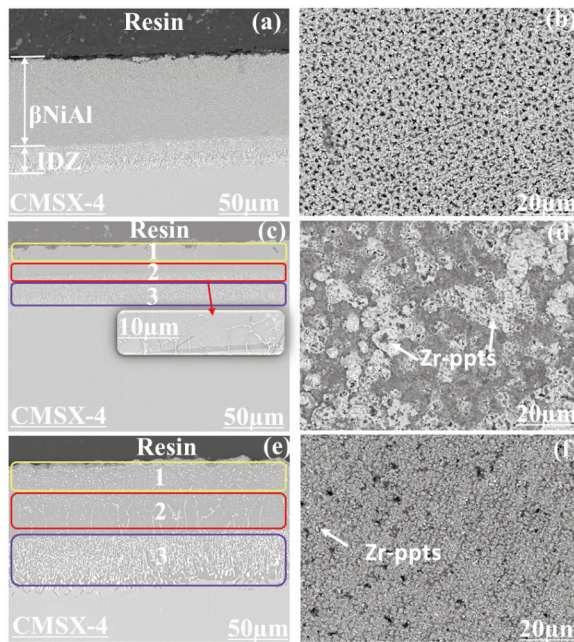
Figure 2. The BSE images of as-deposited BC cross-sections and their surface morphologies; (a) – (b) Zr-free βNiAl, (c) – (d) 1SP, and (e) – (f) 2SPs
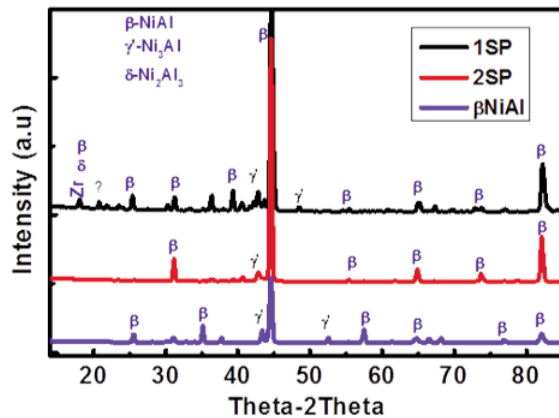

Figure 3. XRD spectrums of Zr-free, 1SP, and 2SP Coatings

Fig. 3 presents the corresponding XRD patterns of BCs that indicated the typical βNiAl peaks as the major phase in all samples. The 1SP revealed the Zr peak, which was consistent with its top surface XRF analysis (see Fig. 2d and Table 1) and no such peak was seen in 2SP. This was due to the low level of Zr on the top surface of 2SP that may not be detected due to XRD sensitivity limitations. The Zr-free BC outer layer consisted of Cr-rich ppts, which also could not be identified by XRD. Because the lattice parameters of α-Cr ppts (seen in Fig. 2b) and βNiAl were closely related, it was hard to distinguish between them [20].

3.1.2. Elastic Modulus and Hardness

The mechanical properties of as-processed Zr doped and undoped coatings were investigated by nano-indentation. Indents were taken on the cross-sections of all coated samples (5 x 4 indents area) using a pyramid-shaped diamond indenter. The average values are presented in Fig. 4. According to initial results, Zr addition, irrespective of Al concentration showed an improvement in the hardness, whereas the elastic modulus of the BCs did not change. Such hardness enhancement was beneficial when coatings were exposed under cyclic oxidation, which minimized rumpling-lead failures. It should be noted here that all these three BCs had the same βNiAl structure, so indents were taken from zones 1 – 3 giving almost identical results. In zone 3 some deviations of values were detected; therefore, the error bars were included to show the standard deviation.
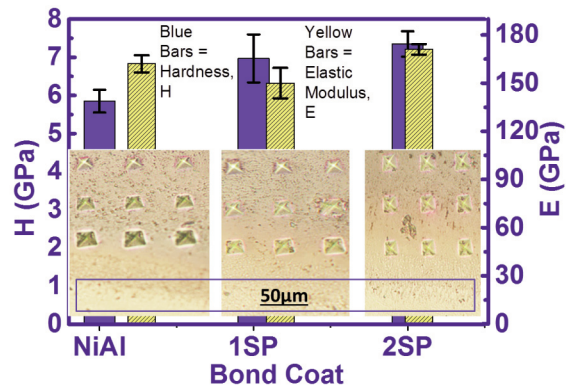

Figure 4. Average hardness and elastic modulus of coatings

3.2. Isothermal Oxidation

Fig. 5a – c presents both SE and BSE micrographs of each oxide and their spalled localities. The Zr-free sample experienced massive spallation as seen in Fig. 5a-BSE. The examination of its spalled locality showed the presence of numerous amounts of refractory rich ppts (table 2). Moreover, Fig. 5a-SE shows the typical ridge morphology of βNiAl.

The worst spallation resistance was shown by 1SP BC as seen in Fig. 5b-BSE. The analysis of its spallation site displayed Zr-rich ppts (Table 2) and oxide morphology was similar to the Zr-free sample as seen in Fig. 5b- SE. On the other hand, 2SP BC experienced the best scale adherence among all BCs and with no typical ridge morphology (Fig. 5c-SE). The location of spallation (Fig. 5c-inset-ii) revealed similar ppts as in 1SP but having a low concentration of Zr and refractory elements (table 2). The Fig. 5c-inset-i picture indicated the Zr-rich pegs into an oxide

that were further confirmed by using EDS mapping of both i.e., oxide surface and cross-sections of 2SP coatings, as shown in Fig. 7. The Zr was seen (green colour in the map) in both the oxide surface (inset) and the oxide-BC interface.
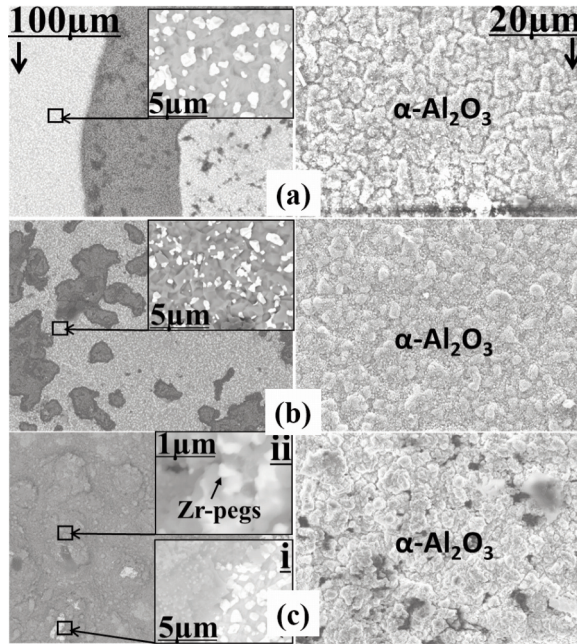

Figure 5. *The oxides morphologies; (a) Zr-free βNiAl, (b) 1SP, and (c) 2SP*
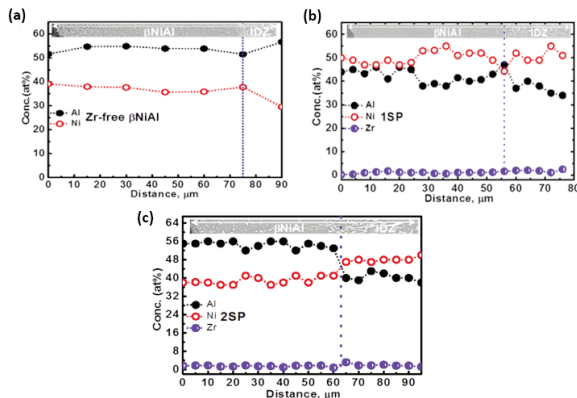

Figure 6. *a) EDS concentration profiles of Zr-free, b) 1SP, and c) 2SP Coatings*

Fig. 6 a – c shows the Al, Ni, and Zr profiles of corresponding BCs obtained by the EDS cross-sectional examinations. It indicated that all BCs were sufficiently rich in Al. The Zr-free and 2SP BC were identical in terms of Al contents, as seen in Fig. 6 b and c, respectively. Whereas an identical amount of Zr could be seen in both 1SP and 2SP, but higher Al amount was detected in later. In addition to EDS, the XRF analysis showed higher Ti, Cr, Co, and W in Zr-

free βNiAl compared to both 1SP and 2SP BCs, as shown in Table 1.

Table 1. *The average composition (at %) of as-deposited BCs*

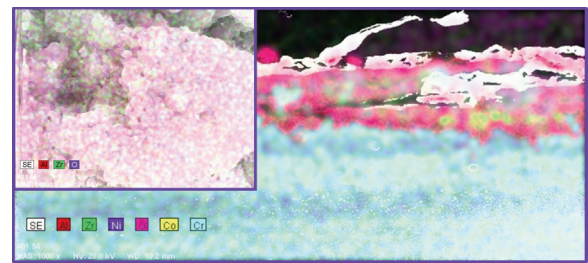|	Al	Zr	Cr	Ti	Mo	Co	W	Ni
βNiAl	51.0	--	3.00	2.00	0.20	4.00	2.50	=
1SP	45.0	1.00	1.50	0.20	--	2.78	0.12	=
2SP	53.0	1.00	1.80	0.30	0.04	2.50	0.26	=
Zr-ppts	33.5	6.30	5.50	--	--	6.60	--	=
Cr-ppts	15.0	--	22	1.50	--	12.0	9.0	=

Figure 7. *EDS elemental mapping of 2SP oxide surface (inset) and scale-BC cross-section*

Table 2. *Composition (at%) of spalled localities of BCs after oxidation*

	Al	Zr	Cr	Ti	Co	W	Re	Ni
βNiAl	7.00	--	19.50	1.00	16.30	15.80	13.70	Remaining
1SP	22.0	17.0	8.70	1.00	9.00	--	--	=
2SP	34.5	2.50	4.00	0.80	6.40	--	--	=

Furthermore, TG analyses were conducted using Setaram Thermo-balance for the determination of the scale growth rates. The growth rates were in
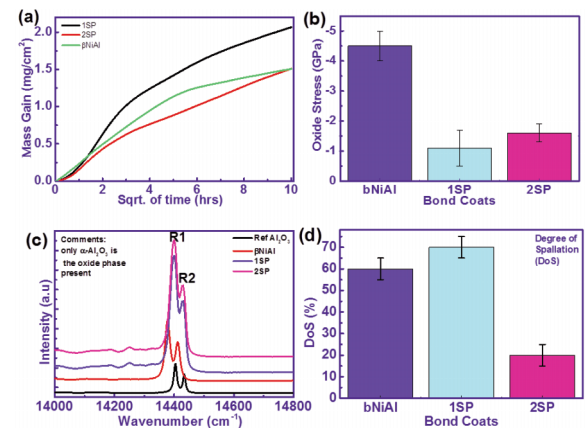

Figure 8. *a)Thermo-gravimetric plots (TG) of Zr-free βNiAl, 1SP, and 2SP samples oxidized at 1150oC for 100 hours in laboratory air. While b-d represents their corresponding oxide stresses, phases, and degree of spallation (DoS), respectively*

increasing order i.e. 1SP>βNiAl>2SP, as shown in Fig. 8a. Therefore, the lowest mass gain was recorded in 2SP and highest in 1SP BC. The Raman examination of intact scales showed residual stresses in the following order βNiAl>2SP>1SP (see Fig. 8b). The lowest compressive stresses were observed in 1SP due to cracking and spallation, which presumably released if any existed. Furthermore, all BCs showed the α-Al$_2$O$_3$ as the only oxide phase after oxidation as shown in Fig. 8c. This occurred because the temperature at which oxidation was carried out triggered the only stable phase i.e., α-Al$_2$O$_3$ since all other transient crystal phases existed under low temperature ranges i.e., < 900 °C (as they were unstable at selected temperature). Therefore, after the oxidation, α-Al$_2$O$_3$ was the only phase in Al-enriched bond coats as evident from the literature. However, once aluminium was consumed to the level when β to β' transformation began as noted established in Al-Ni binary diagram causing the growth of other oxides i.e., NiO, TiO$_2$ etc.

The degree of spallation was calculated (see Fig. 8d) by taking into account the total scale surface area, which was in the following order 2SP>βNiAl>1SP (Fig. 8d).

The after-oxidation cross-sections were analysed to understand the after-oxidation effects on BC in terms of its stability. Fig. 9 shows the cross-section of BC after oxidation. The interfacial voids and γ' phase (~30%) were visible on the top of the cross-section in Zr-free BC as shown in Fig. 9a. Oxide did not retain due to massive spallation and the rest of the attached oxide was damaged during sample preparation. Interestingly, massive βNiAl – γ'-Ni3Al phase transformation was observed in 1SP (~90%) as indicated in Fig. 9b. Moreover, thick alumina with white particles showing spinels was distinctly visible in addition to interfacial pores. The 2SP showed extremely localized β – γ' transformation (< 5%), minimal voids, and thin Al$_2$O$_3$ layer as shown in Fig.
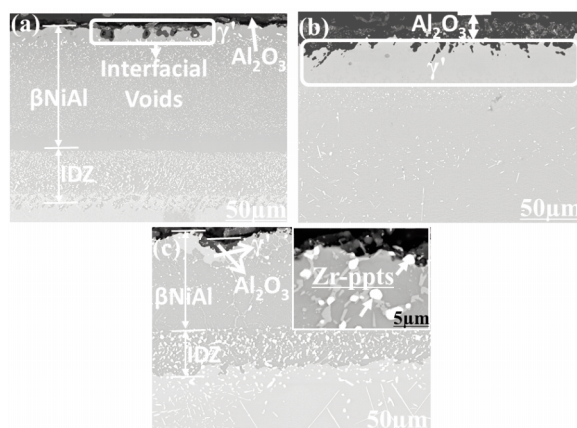

***Figure 9.** After oxidation cross-sections (BSE mode); (a) Zr-free βNiAl, (b) 1SP, and (c) 2SP*

9c. The figure inset image showed the presence of Zr into ppts alongside βNiAl grain boundaries.

4. Discussion

This study aimed to dope Zr uniformly into βNiAl coatings and to investigate its beneficial effects as an alternative BC. Previous works on Zr addition was done by either using PVD or CVD [21-23], but few ones utilized pack aluminizing with little or no success to the best of our knowledge. All major publications were on bulk materials [24, 25], which greatly differed from coatings. Thus, the present study developed the fabrication methods of Zr-doped BC and investigated its oxidation performance and mechanisms of its beneficial effects.

4.1. BC Processing Aspects

Firstly, both single and multiple step pack aluminizing methods successfully doped Zr into βNiAl coatings. Initially, co-deposition of Zr and Al were carried out in a single step, but lower Al and Zr contents and particularly higher Zr enrichment on the surface were its major drawbacks. This was due to differences in partial pressures of aluminium chloride and zirconium chloride and the limited solid solubility of Zr dopant in the substrate and βNiAl coatings. To overcome such problems two steps of aluminizing was adopted. Interestingly, higher contents of Al and Zr were observed in the βNiAl layer with minimum content on the surface (see Fig. 2d). It was because of the processes' first step that introduced Zr into γ-Ni/γ'-Ni$_3$Al structure of superalloy (see Table 3 and Fig. 10). The REs were more soluble in γ'-Ni$_3$Al compared to βNiAl and γ-Ni. The second step of aluminizing caused the Zr-enriched-γ/γ' to convert into the βNiAl phase, thereby dissolving some of Zr and its excess precipitated out.

Notably, such stepwise deposition had two implications; (1) it allowed higher Zr into substrate and coating interface, thereby inhibiting the substrate out-diffusion (as mentioned in Table 1), which acted as a diffusion barrier, and (2) such ppts caused hardness rise (Fig. 4) of BC possibly by ppt-strengthening, which was beneficial for reducing cyclic plasticity (rumpling in the event of oxidation). Furthermore, it was mandatory to maintain the Zr reservoir that enhanced the nucleation of α-Al$_2$O$_3$ and thereby changing ionic flux [26, 27] during oxidation. Therefore, in addition to Al, 2SP BC contained an adequate amount of Zr required for improved scale adhesion during oxidation. Furthermore, XRD analysis (Fig. 3) showed no new phase formed (or at least not detected). This was due to the extremely low concentration of Zr and its limited solid solubility in aluminide (fractions of 1 at %). Moreover, the XRD

results were in close agreement with EDS and XRF analyses.

Table 3. *Zr-enriched-γ/γ' phase of CMSX4 before aluminizing*

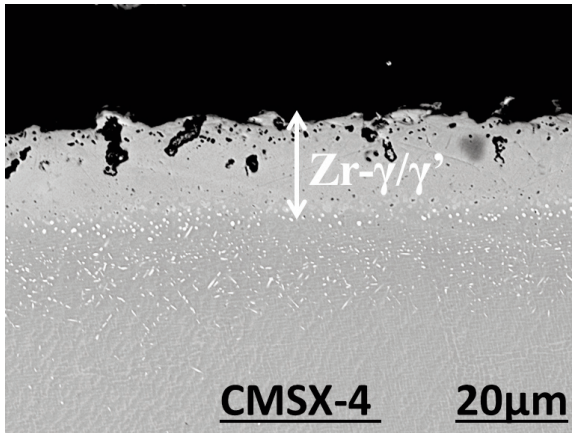| Zr-rich-γ/γ'	Al	Co	Cr	W	Ti	Zr	Ni
(at%)	12.50	11.0	5.3	0.8	1.0	5.5	Remaining

Figure 10. *The cross-sections of as-zirconized CMSX4 in the first step (no aluminizing at this stage). These cross-sections are intentionally placed in the discussion part for an easy understanding of the 2SP process*

Moreover, it is strongly believed that BC residual stresses could promote rumpling [28]. Such stresses are likely to be attained during the cooling cycle of BC fabrication [29] because of the coefficient of thermal expansion (CTE) mismatch. Keeping in mind this sensitive issue, a new approach was adopted, which included diffusion leading stress-relieving treatment (Fig. 1d) after doping. Therefore, enhancement of hardness and elimination of BC stresses [30] are encouraging aspects of REs addition in terms of its mechanical integrity.

4.2. Oxidation Aspects
4.2.1. Zr-free βNiAl

The Zr-free sample showed poor oxide adhesion witnessed by severe spallation, high mass gain, and oxide stress (shown in Fig. 5a/8a – b and d). All of these observations are well established in the literature. Moreover, the generation of interfacial voids (Fig. 9a) was due to fast Al depletion by both inward towards the substrate and outward to oxide. Such voids reduce the effective area for oxide adhesion, and hence allow speedy spallation. Also, the rise in overall BC thickness (see Fig. 9a) that indicated massive interdiffusion, particularly out-diffusion of substrate elements into the coating, which further diluted or destabilized the β structure.

Interestingly, one major cause of spallation was the refractory (W, Ta, Co, Cr, Ti, etc.) rich ppts found at the oxide/coating interface (shown in Fig. 5a-inset). Such accumulation of refractory rich precipitates underneath the oxide compromised its adhesion to coating thereby causing cracking and eventual spallation due to their fast growth.

4.2.2. 1SP

The 1SP showed the worst oxide adhesion among all BCs by experiencing massive spallation.

The examination of spallation sites witnessed a large number of Zr-rich refractory ppts. It should be noted that pre-oxidation XRF and EDS analyses witnessed high Zr on the surface and low in cross-sections. The post-oxidation cross-section observation indicated severe β – γ' phase transformation. This potentially was due to an excessive Zr on the surface (Fig. 2d) in as processed condition, which was an active metal that oxidized coating faster and increased the oxide growth rates, and induced cracking. The high oxide growth depleted Al quickly and destabilized β structure as observed in Fig. 8b. More importantly, the lower initial (as processed) Al content exaggerated the Zr effect, which was also termed as over-doping [17, 25, 31]. As 1 at % Zr in BC was an amount that fell in the category of over-doping especially when the percentage of Al was low. Recent studies demonstrated that higher Al content (~50 at%) enhanced the oxidation resistance even with high Zr (1 at%) [23]. In terms of BC stability over-doping accelerated Al depletion and hence, speedy β-γ' phase transformation was observed (also spinel particles in scale were seen) [24, 32, 33]. Thus, lower Al (Table 1) in 1SP caused Zr to dominate the oxidation process along with other elements, e.g., Ti, Cr, and Ni. Moreover, the intact oxide (Fig. 5b-SE image) was similar to Zr-free undoped sample (even rougher). This implied that there was no beneficial effect of doping Zr into the BC, as it caused poor spallation resistance in comparison with Zr-free samples.

4.2.3. 2SP

The adhesion of BC is a core performance indicator, which expresses how well it performs under aggressive oxidizing environments. The spallation resistance is a complex interplay of numerous factors. The dominant ones are the scale growth and stresses, BC stability (Al depletion either inward or outward), and interdiffusion effects (by substrate-BC). These parameters were elaborated in the present work. The mass gain plots shown earlier (Fig. 8(a)) indicated the lowest growth rate and spallation (Fig. 5c) by the 2SP sample. Such low growth reduced the oxide thickening. Furthermore, Zr was present in oxide

forms, and therefore the Zr-pegs extending to the BC interface inter-locking it (Fig. 5c-inset-i and Fig. 7). Such oxide pegging proved to enhance the spallation resistance [17]. During oxidation, Zr tended to migrate via βNiAl grain boundaries (Fig. 9c-inset) [34] and passed through an oxide-coating interface, and finally segregating at oxide grain boundaries [17]. To understand the implications of such movement, oxygen tracer studies confirmed that characteristic counter flow of cations (Al^{+3}) and anions (O^{-2}) in undoped βNiAl BC dominated the oxidation process thereby enhancing its growth rates. However, when Zr was doped into BC, the typical ionic transport changed [17, 35]. Zr promoted anionic (O^{-2}) transport (and impeding Al^{+3} flows to scale) during oxidation occurred, reducing oxide growth as a consequence (seen in Fig. 8a), and hence attainment of stresses (Fig. 8b). Also, the rate of anionic diffusion was slower and as a result the reduction in scale growth rate was achieved [36]. It is well known that Al depletion causes BC destabilization. The ionic radius of Zr was significantly higher than that of Al, and during oxidation, it migrated upward. It minimized the outward migration of Al cations passing through BC and also impeded the inward Al depletion to the substrate. Such dual effects by Zr predominately decreased the overall Al departure in both ways, and hence stabilized BC. The slow movement of Zr ions to the BC-oxide interface and onward, hindered the bypassing substrate elements making oxide clean too (unpublished data). It was believed that oxide morphologies changed when REs were added into BC, as the oxidation process was dominated by anions lead preferential growth. The typical ridge morphology was obtained in Zr-free βNiAl [7, 24], which changed by the addition of Zr into less distinctive or fewer ridges (seen in Fig. 5c-SE image). The elimination or reduction of interfacial voids further confirmed that Zr suppressed the vacancies [24] by reducing the Al transport and Ni departure due to its slow ionic migration. This minimized the diffusion imbalance, which was responsible for voids formation [27]. In general, the stoichiometric content of Al was equally mandatory as Zr doping. The overall Zr content was the same in both 1SP and 2SP BCs, but richer in Al in the former. Lower Al content, on the other hand, resulted in the poor performance of sample 1SP. Recent studies have demonstrated that higher Al content (~ 50 at%) enhanced the oxidation resistance even with high Zr (1 at%) [23]. In contrast, low Al and high Zr were detrimental for the oxidation life of the BC, as established in the 1SP sample.

5. Conclusions

Based on initial results, it was demonstrated that pack aluminizing could be successfully utilized for doping of REs and could introduce even higher Zr into Cr-rich ppts. The Zr addition improved BC hardness and diffusion of substrate elements. The isothermal oxidation tests revealed improved scale adhesion and its slow growth with minimum oxide stresses. Moreover, Zr doping made the BC slightly diffusion barrier by reducing both inward and outward elemental migration and hence stabilizing the βNiAl structure. Nevertheless, it is mandatory to maintain sufficient Al alongside Zr for optimized spallation resistance. Furthermore, over-doping either locally or into the entire sample destabilized the βNiAl structure thereby compromising oxide adhesion by forming refractory rich fast-growing ppts (and spinels).

Acknowledgement

References

[1] N. Birks, G. Meier, F. Pettit, JOM, 46 (12) (1994) 42 - 46 .

[2] R. Mévrel, Mater. Sci. Eng., A, 120 (1989) 13 -24.

[3] J.A. Haynes, M. Ferber, W. Porter, J. Therm. Spray Technol., 9 (1) (2000) 38 - 48.

[4] A. Maricocchi, A. Bartz, D. Wortman, J. Therm. Spray Technol., 6 (2) (1997) 193 - 198.

[5] J. Nicholls, JOM, 52 (1) (2000) 28-35.

[6] M. Gell, K. Vaidyanathan, B. Barber, E. Jordan, J. Cheng, Metall. Mater. Trans. A, 30 (2) (1999) 427 - 435.

[7] B. A. Pint, J. R. Martin, L.W. Hobbs, Oxid. Met, 39 (3-4) (1993) 167 - 195.

[8] D.R. Clarke, C.G. Levi, Annu. Rev. Mater. Res., 33 (1) (2003) 383 - 417.

[9] B. Sudhangshu, High Temperature Coatings, Elsevier, Burlington, (2007) 73.

[10] L.P. Andrew, M.W. Bruce, Surf. Coat. Technol., 146-147 (2001) 1 - 6.

[11] J. Haynes, B.A. Pint, Y. Zhang, I.G. Wright, Surf. Coat. Technol., 202 (4-7) (2007) 730 - 734.

[12] H. Tawancy, N.M. Abbas, T.N. Rhys-Jones, Surf. Coat. Technol., 49 (1-3) (1991) 1 - 7.

[13] H. Tawancy, N. Sridhar, N.M. Abbas, D. Rickerby, Scr. Metall., 33 (9) (1995) 1431 - 1438.

[14] B.M. Warnes, D.C. Punola, Surf. Coat. Technol., 94-95 (1997) 1 - 6.

[15] Y. Zhang, W.Y. Lee, J.A. Haynes, I.G. Wright, B.A. Pint, K.M. Cooley, P.K. Liaw, Metall. Mater. Trans. A, 30A (10) (1999) 2679-2687.

[16] B. Pint, K. More, I. Wright, P. Tortorelli, Mater. High

Temp., 17 (1) (2000) 165-171.

[17] B. A. Pint, Oxid. Met., 45 (1-2) (1996) 1-37.

[18] J. G. Smeggil, Mater Sci. Eng., 87 (1987) 261-265.

[19] D.P. Whittle, J. Stringer, Philos. Trans. R. Soc. London, Ser. A, 295 (1413) (1980) 309 - 329.

[20] Cr, ICDD file No. 00-006-0694. Newtown Square, PA: International Centre for Diffraction Data; 2010.

[21] M. Zagula-Yavorska, J. Romanowska, Arch. Mater. Sci. Eng., 58 (2) (2012) 250 - 254.

[22] S. Hamadi, M.P. Bacos, M. Poulain, A. Seyeux, V. Maurice, P. Marcus, Surf. Coat. Technol., 204 (6–7) (2009) 756 - 760.

[23] J.R. Brian, G. Mark, B. Brett, D. Ram, TMS, (2008) 753 - 760.

[24] D. Li, G. Hongbo, W. Di, Z. Tian, G. Shengkai, X. Huibin, Corros. Sci., 66 (0) (2013) 125 - 135.

[25] B.A. Pint, Oxid. Met., 49 (5/6) (1998).

[26] B.A. Pint, I.G. Wright, W.Y. Lee, Y. Zhang, K. Prüßner, K.B. Alexander, Mater. Sci. Eng., A, 245 (2) (1998)

201 - 211.

[27] H.J. Grabke, Intermetallics, 7 (10) (1999) 1153 - 1158.

[28] A.W. Davis, A.G. Evans, Metall. Mater. Trans. A, 37 (7) (2006) 2085 - 2095.

[29] M. Watanabe, D.R. Mumm, S. Chiras, A.G. Evans, Scr. Mater., 46 (1) (2002) 67 - 70.

[30] A.D. Chandio, Key Eng. Mater., 875 (2021) 280 - 285.

[31] J.D. Kuenzly, D.L. Douglass, Oxid. Met., 8 (3) (1974) 139 - 178.

[32] S. Wang, J. He, H. Song, S. Liang, H. Peng, H. Guo, Coatings, 10 (9) (2020) 874.

[33] H. Guo, L. Sun, H. Li, S. Gong, Thin Solid Films, 516 (16) (2008) 5732 - 5735.

[34] D.J. Larson, M.K. Miller, Mater. Charact., 44 (1-2) (2000) 159 - 176.

[35] C. Céline, S. Chevalier, Y. Cadoret, Mater. Sci. Forum, 595-598 (2008) 41 - 49.

[36] M.S. Li, P.Y. Hou, Acta Mater., 55 (2) (2007) 443 - 453.

OBRADA, KARAKTERIZACIJA I OTPORNOST NA OKSIDACIJU KOD βNiAl VEZIVNE PREVLAKE: UTICAJ Al I Zr

A.D. Chandio [a,*], A.A. Shaikh [b], W. Salman [c], H. Ahmed [a]

[a] NED Univerzitet za inženjerstvo i tehnologiju, Fakultet za metalurško inženjerstvo, Pakistan
[b] NED Univerzitet za inženjerstvo i tehnologiju, Fakultet za hemijsko i procesno inženjerstvo, Pakistan
[c] Severozapadni politehnički univerzitet, Glavna državna laboratorija za ispitivanje očvršćavanja, Fakultet za nauku o materijalima i inženjerstvo, Kina

Apstrakt

βNiAl vezivna prevlaka modifikovana platinom je materijal koji se koristi kao termička prevlaka kod vazduhoplovnih motora za smanjenje temperature na površini motora. Međutim, poželjno je smanjiti troškove proizvodnje i materijala nalaženjem pristupačnije alternative sličnih performansi. Poznato je da bi manja koncentarcija reaktivnih elemenata, kao što su Zr, Hf and Y, mogla značajno poboljšati adheziju oksida, u određenim slučajevima i bolje od materijala modifikovanih platinom. Cilj ovog rada je dizajniranje i izrada βNiAl vezivne prevlake modifikovane cirkonijumom na superleguri CMSX-4 primenom metode aluminizacija. Pored toga, ispitivanje se bavilo i razvijanjem sistematskog razumevanja osnovnih mehanizama koji stoje iza pozitivnih efekata upotrebe reaktivnih elemenata. Pripremljena su tri seta vezivnih prevlaka: βNiAl bez Zr (bez primesa), set sa Al i Zr koji su dodati postupkom koji je sadržao jedan korak (1SP) i set sa Zr i Al koji su pojedinačno dodati u postupku koji je sastojao od dva koraka (2SP) – cirkonizacija i aluminizacija. Takva tri seta vezivnih prevlaka su omogućila razumevanje načina obrade, kao i efekte Zr i Al na stepen adhezije. Konkretno, setovi 1SP i 2SP su pokazali da se Zr podjednako nataložio i stvorio mrežu koja je doprinela povećanju tvrdoće. Svi vezivne prevlake su izotermički oksidovale na 1150 ºC tokom 100 sati, pri čemu je 2SP pokazao najbolju otpornost na spalaciju (raspadanje) i mikrostrukturnu stabilnost, a njegov oksidni sloj koji je sadržao Zr se prostirao do podloge. Pored uticaja Zr, dokazano je da je sadržaj Al u vezivnoj prevlaci jednako uticao na adheziju oksida. Kada je sadržaj Zr bio isti (1SP i 2SP = 1at %), set sa većim sadržajem Al pokazao je bolju otpornost na spalaciju (raspadanje), dok je niži sadržaj Al prouzrokovao obrnuti efekat zbog reaktivne prirode Zr koji je nazvan prekomerni doping. Utvrđeno je da se prekomerni doping dogodio ili lokalno ili preko celog vezivnog premaza, što je dovelo do ubrzanog iscrpljivanja Al koje je prouzrokovalo destabilizaciju prelaska βNiAl u γ'-Ni3Al fazu. Dobijeni rezultati se predstavljeni i opsežno se diskutovalo o njima.

Ključne reči: βNiAl vezivna prevlaka; Otpornost na oksidaciju; Termička prevlaka; Dodavanje reaktivnih elemenata; Aluminizacija